Fast Classification and Depth Estimation for Multispectral Single-Photon LiDAR Data

Fast Classification and Depth Estimation for Multispectral Single-Photon LiDAR Data

Mohamed Amir Alaa Belmekki, Stephen McLaughlin, Abderrahim Halimi
School of Engineering and Physical Sciences, Heriot-Watt University, Edinburgh U.K.

***Abstract*—Multispectral 3D LiDAR imaging plays an important role in the remote sensing community as it can provide rich spectral and depth information from targets. This paper proposes a fast pixel-wise classification algorithm for multispectral single-photon LiDAR imaging. The algorithm allows the detection of histograms containing surfaces with specific spectral signatures (i.e., specific materials) and discarding those histograms without reflective surfaces. The proposed Bayesian model is carefully built to allow the marginalization of latent variables leading to a tractable formulation and fast estimation of the parameters of interest, together with their uncertainties. Results on simulated and real single-photon data illustrates the robustness and good performance of this approach.**

***Index Terms*—3D Multispectral imaging, Single-photon LiDAR, Bayesian estimation, Poisson statistics, Multispectral classification.**

I. Introduction

Light detection and ranging (LiDAR) used with a time-correlated single-photon detector has received increased attention in the scientific community over the last few decades in numerous applications such as defence, automotive [1], and environmental sciences [2]. It has successfully proven its efficiency for long-range depth imaging [3]–[5], depth imaging in turbid media [6]–[8] and multispectral imaging [9], [10]. A multispectral LiDAR system operates by illuminating the scene using laser pulses of different wavelengths and recording the arrival times of the reflected photons using a time-correlated single-photon counting (TCSPC) module. A histogram of photon counts with respect to time-of-flight is constructed for each pixel and wavelength. The resulting histograms contain information regarding the object depth profile and its spectral signature (i.e., reflectivity at each wavelength). When the number of spectral bands considered is large enough, it becomes possible to identify and quantify the main materials in the scene, in addition to estimating classical LiDAR-based range profiles.

In the last decade, many works were published promoting the use of multiple wavelengths in LiDAR imaging as it allows robust restoration of the range and spectral profile of the target [10]–[12], spectral classification [13] and spectral unmixing [9], [14]. In [13], joint depth estimation and spectral classification using multispectral 3D LiDAR have been proposed. The algorithm combined a Bayesian model with a Markov chain Monte-Carlo (MCMC) sampling strategy to obtain estimates and their uncertainties. However, the algorithm assumed the absence of background counts due to ambient light, and has a significant computational cost due to the considered MCMC sampling method, which is incompatible with real-time requirements. A faster algorithm was proposed in [9] by considering an optimization algorithm to estimate a depth image and spatially unmix the contribution of different materials. However, the method did not quantify the estimates uncertainty, as often required for decision making. Recently, two fast algorithms were introduced in [15], [16] to perform target detection task using 3D Lidar imaging. These two algorithms use a Bayesian formulation and show state-of-the-art performance even under the presence of background illumination. Nevertheless, these two algorithms are not able to discern between different materials having distinctive spectral responses.

This paper proposes a new fast algorithm for per-pixel multispectral classification and range estimation, while also providing uncertainty measures about the estimates. Assuming a known spectral library of different materials, the proposed Bayesian strategy allows the detection of pixels with reflections from a target, and to identify the target material based on the known signatures. The proposed algorithm operates on histograms of counts and assumes the presence of at most one surface per-pixel. The model accounts for the Poisson statistics of the data to define the likelihood, and considers suitable prior distributions for the parameters of interest. The resulting marginalized posterior distribution can be efficiently exploited allowing parameters estimation together with uncertainty quantification. The proposed algorithm can be used to compress the high-volume multispectral data by withdrawing uninformative pixels without surfaces/objects. It can also be used as a target detection algorithm to spatially locate materials with specific spectral signatures, e.g., the detection of man-made objects in turbid environments such as metallic objects underwater. The proposed algorithm is tested both on real and simulated data showing promising results even in the sparse photon regime or in presence of a high background level of counts.

The paper is structured as follows. Section II introduces the multispectral LiDAR observation model. The classification problem formulation using Bayesian framework and the estimation strategy are presented in Section III and Section IV, respectively. Results on simulated and real data are presented in Section V. Conclusions and future work are finally reported in Section VI.

II. Observation model

We consider a 3-dimensional cube of histograms $\boldsymbol{Y}$ of LiDAR photon counts of dimension $N \times L \times T$, where N is the number of scanned spatial positions (i.e., pixels), L is

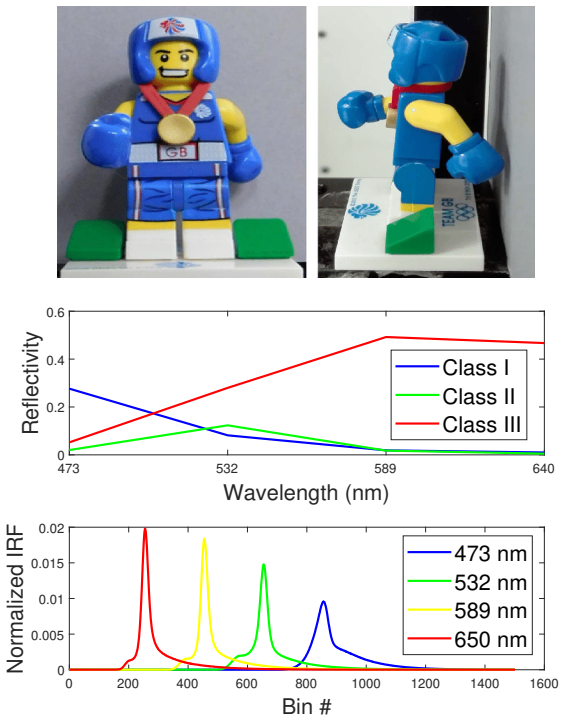

Fig. 1. (Up) The considered scene used in section V, (middle) spectral signatures of the spectral classes associated with Lego scene, (down) the normalized IRFs associated with the wavelengths 473, 532, 589 and 640 nm [19] used in Section V

the number of spectral wavelengths and T is the number of time bins. Let $\boldsymbol{Y}_n = [\boldsymbol{y}_{n,1}, \boldsymbol{y}_{n,2}, ..., \boldsymbol{y}_{n,L}]^T$ be an $L \times T$ matrix where $\boldsymbol{y}_{n,l} = [y_{n,l,1}, y_{n,l,2}, ..., y_{n,l,T}]^T$. According to [17], [18], each photon count $y_{n,l,t}$, where $n \in \{1, ..., N\}$, $l \in \{1, ..., L\}$ and $t \in \{1, ..., T\}$, is assumed to follow a Poisson distribution as follows

$$y_{n,l,t}|r_{n,l}, d_n, b_{n,l} \sim \mathcal{P}[r_{n,l}\, g_l(t - d_n) + b_{n,l}], \qquad (1)$$

where $\mathcal{P}(.)$ denotes a Poisson distribution, $r_{n,l} \geq 0$ is the spectral signature observed at the l_{th} wavelength, $d_n \in \{1, 2, ..., T\}$ represents the position of an object surface at a given range from the sensor, $b_{n,l} \geq 0$ is the constant background level associated with dark counts and ambient illumination and $g_l(.)$ is the system impulse response function (IRF), whose shape can differ between wavelength channels (see Fig.1), assumed to be known from a calibration step and normalized $\sum_{t=1}^{T} g_l(t) = 1$. An equivalent model can be considered as in [15] using the signal-to-background ratio (SBR), which is defined as the ratio of the useful detected photons $r_{n,l}$ and the total number of background photons in the histogram $b_{n,l}T$, i.e.: $w_{n,l} = \frac{r_{n,l}}{b_{n,l}T}$ with $w_{n,l} \geq 0$. Thus, (1) can be written in the following form

$$y_{n,l,t}|\omega_{n,l}, d_n, b_{n,l} \sim \mathcal{P}\{b_{n,l}\,[w_{n,l}\,T\, g_l(t - d_n) + 1]\}. \qquad (2)$$

This new formulation is interesting as it allows an easy marginalization of the posterior distribution with respect to (w.r.t.) the background noise parameter as indicated in Section III. Under the assumption that all the observed pixels, wavelengths and bins are mutually independent, the joint likelihood can be written in the following form:

$$p(y_{n,l,t}|\omega_{n,l}, d_n, b_{n,l}) = \prod_{l=1}^{L}\prod_{t=1}^{T} p(y_{n,l,t}|\omega_{n,l}, d_n, b_{n,l}). \qquad (3)$$

Our goal is to perform pixel classification based on an available database of spectral signatures. As a result, the classification task will require an elaborated strategy to mitigate the unknown $b_{n,l}, \omega_{n,l}$ and d_n parameters.

III. Hierarchical Bayesian model for classification

The classification problem is an ill-posed problem that is tackled by considering a Bayesian approach. The latter assigns prior distributions for the unknown parameters to regularize the inverse-problem.

A. Prior distributions

A Lidar histogram can either result from background counts (in absence of a target photons due to $r_n = \omega_n = 0$) or a mixture of target and background counts (when $r_n \geq 0$ or $\omega_n \geq 0$). Assuming the presence of K spectral signatures, the classification problem aims to associate a pixel with a target to one of the K spectral classes. The reflectivity prior accounts for this effect by considering a mixture of $K + 1$ distributions as follows

$$P(r_{n,l}|u_n, \alpha^r_{k,l}, \beta^r_{k,l}, K) = \delta(u_n)\delta(r_{n,l}) + \sum_{k=1}^{K} \delta(u_n - k)\mathcal{G}(r_{n,l}; \alpha^r_{k,l}, \beta^r_{k,l}) \qquad (4)$$

where $u_n \in \{0, 1, ..., K\}$ is a latent variable that indicates the absence of target if $u_n = 0$, otherwise, it indicates the label of the class, $\delta(.)$ is the Dirac delta distribution centred in 0, $\mathcal{G}(r_{n,l}; \alpha^r_{k,l}, \beta^r_{k,l})$ represents a gamma density whose shape and scale hyperparameters $\left(\alpha^r_{k,l}, \beta^r_{k,l}\right)$ are fixed based on the K known spectral signatures. This prior is inspired from the spike-and-slab prior used in [15]. It accounts for $K + 1$ cases, the first represents the absence of a target in the the nth pixel and is obtained for $u_n = r_{n,l} = 0$, hence the use of a Dirac distribution (the spike part). The slab part accounts for the presence of one of the K signatures by using a gamma distribution. Thanks to the use of many wavelengths, this prior extends the object detection problem in [15] to a class detection problem using the spectral signature of each class.

Considering the non-negativity of $b_{n,l}$, $\forall n, l$ and its continuous nature, the background level will be modelled with a gamma distribution as in [20]:

$$P(b_{n,l}|\alpha^b_l, \beta^b_l) = \mathcal{G}(b_l, \alpha^b_l, \beta^b_l) \qquad (5)$$

where α^b_l and β^b_l are background hyper-parameters. Considering that only dozens of distinctive wavelengths will be used, we will consider the channels to be uncorrelated to keep the estimation strategy tractable. Since we are interested in using the model described in (2) instead of (1), assuming that the reflectivity and the background noise are independent and by applying a random variable change, the resulting joint prior distribution will yield:

$$p(\boldsymbol{\omega_n}, \boldsymbol{b_n}|u_n, \boldsymbol{\phi}, K) = \prod_{l=1}^{L} p(\omega_{n,l}, b_{n,l}|u_n, \phi_l)$$
$$= \prod_{l=1}^{L} \Big[\delta(u_n)\delta(\omega_{n,l})\mathcal{G}(b_{n,l}, \alpha_l^b, \beta_l^b) + \sum_{k=1}^{K} \delta(u_n - k) C_{k,l}(\omega_{n,l})\mathcal{G}(b_{n,l}, \alpha_{l,k}^{\dagger}, \beta_{l,k}^{\dagger}(\omega_{n,l}))\Big] \quad (6)$$

with

$$C_{k,l}(\omega_{n,l}) = \frac{(\beta_l^b)^{\alpha_l^b}(\beta_{k,l}^r)^{\alpha_{k,l}^r} T^{\alpha_{k,l}^r}}{B(\alpha_{k,l}^r, \alpha_l^b)} \frac{\omega_{n,l}^{\alpha_{k,l}^r - 1}}{\beta_{l,k}^{\dagger}(\omega_{n,l})^{\alpha_{l,k}^{\dagger}}}$$

$$\alpha_{l,k}^{\dagger} = \alpha_l^b + \alpha_{k,l}^r$$

$$\beta_{l,k}^{\dagger}(\omega_{n,l}) = \beta_l^b + \beta_{k,l}^r T \omega_{n,l}$$

where $B(.)$ is the beta function and $\boldsymbol{\phi} = (\phi_1, \phi_2, ..., \phi_l)$ with $\phi_l = (\alpha_{k,l}^r, \beta_{k,l}^r, \alpha_l^b, \beta_l^b)$, $k \in \{0, ..., K\}$.

As we suppose that we have no prior knowledge about a pixel's class, the parameter u_n is assumed to be drawn from a uniform distribution, i.e.: $p(u_n = k) = \frac{1}{K+1}$, where $k \in \{0, ..., K\}$. However, This non-informative class prior can be changed in presence of additional information regarding the classes. The depth parameter d_n is assigned a non-informative uniform prior as follows:

$$p(d_n = t) = \frac{1}{T} \quad , \forall t \in \{1, ..., T\}. \quad (7)$$

Nonetheless, this can be modified in case of additional information regarding the target position.

B. Joint Posterior distribution

From the joint likelihood in equation (3) derived in Section II and the prior distributions specified in Section III-A, we can obtain the joint posterior distribution for $\boldsymbol{\omega_n}$,$\boldsymbol{b_n}$, d_n and u_n given the 3D histograms $\boldsymbol{Y_n}$ and the hyperparameters $\boldsymbol{\phi}$ and K. Using Bayes rule and assuming that d_n and u_n are independent from $\boldsymbol{\omega_n}$ and $\boldsymbol{b_n}$, the joint posterior distribution of the proposed Bayesian model can be formulated in the following form:

$$p(\boldsymbol{\Theta_n}|\boldsymbol{Y_n}, \boldsymbol{\phi}, K) \propto p(\boldsymbol{Y_n}|\boldsymbol{\Theta_n}) p(\boldsymbol{\Theta_n}|\boldsymbol{\phi}, K) \quad (8)$$

where

$$\boldsymbol{\Theta_n} = (\boldsymbol{\omega_n}, \boldsymbol{b_n}, d_n, u_n)$$

$$p(\boldsymbol{\Theta_n}|\boldsymbol{\phi}, K) = p(\boldsymbol{\omega_n}, \boldsymbol{b_n}, d_n, u_n|\boldsymbol{\phi}, K)$$
$$= p(\boldsymbol{\omega_n}, \boldsymbol{b_n}|\boldsymbol{\phi}, u_n, K) p(d_n) p(u_n). \quad (9)$$

IV. ESTIMATION STRATEGY

The posterior distribution in (8) reflects our knowledge of the unknown parameters to be estimated given the photon data and the available prior knowledge. The Bayesian estimator to be considered, both for the depth and class parameter, is the maximum a posteriori (MAP) estimator as in [9], [14]. From equation (8), we marginalize the background noise and signal-to-background parameters to get the joint depth and class marginal probability as follows:

$$p(u_n, d_n|\boldsymbol{Y_n}) = \int\int p(\boldsymbol{\omega_n}, \boldsymbol{b_n}, d_n, u_n|\boldsymbol{Y_n}) d\boldsymbol{b_n}\, d\boldsymbol{\omega_n} \quad (10)$$

A. Class estimation

The following decision rule is adopted to determine the pixel label

$$H_n = \max_{k=1:K} p(u_n = k \,|\, \boldsymbol{Y_n}) \quad (11)$$

with

$$p(u_n|\boldsymbol{Y_n}) = \sum_{d_n=1}^{T} \int\int p(\boldsymbol{\omega_n}, \boldsymbol{b_n}, d_n, u_n|\boldsymbol{Y_n}) d\boldsymbol{b_n}\, d\boldsymbol{\omega_n} \quad (12)$$

where H_n represents the class of the n^{th} pixel . Note that for $K = 1$ and $L = 1$, we end up with a target detection decision rule as in [15]. We demonstrate that the marginal probability $p(u_n|y_n)$ is :

$$p(u_n = k|\boldsymbol{Y_n}) = \sum_{d_n=1}^{T} \int_0^{\infty} \prod_{l=1}^{L} \big[p(u_n = k) p(d_n) D_{n,l,k} \gamma_l^{-1} F_{n,l,k}(\omega_{n,l}, d_n) d\omega_{n,l}\big] \quad (13)$$

with

$$\gamma_l = \frac{\Gamma(\alpha_l^b)}{(\beta_l^b)^{\alpha_l^b}} \prod_{t=1}^{T} y_{n,l,t}!$$

$$D_{n,l,k} = \frac{\Gamma(\bar{y}_{n,l} + \alpha_l^b + \alpha_{k,l}^r)(T\beta_{k,l}^r)^{\alpha_{k,l}^r}}{\Gamma(\alpha_{k,l}^r)}$$

$$F_{n,l,k}(\omega_{n,l}, d_n) = \frac{\exp\{\sum_{t=1}^{T} y_{n,l,t} \ln[\omega_{n,l} T g_l(t - d_n) + 1]\}}{\omega_{n,l}^{1-\alpha_{k,l}^r} \{\beta_l^b + [T(1 + \omega_{n,l}(1 + \beta_{k,l}^r))]\}^{\alpha_{l,k}^{\dagger} + \bar{y}_{n,l}}} \quad (14)$$

where $\bar{y}_{n,l} = \sum_{t=1}^{T} y_{n,l,t}$. In the event of no target, we can see that the integral is available in its analytical form thanks to the conjugacy between the model (2) and the priors (6). The marginal distribution in (13), however, is intractable. One way to simplify it is to consider that the depth captured is different across all the spectral wavelengths. This simplification improves the tractability of the marginal class probability and will transform (13) into (15) as follows:

$$p(u_n = k|\boldsymbol{Y_n}) = \prod_{l=1}^{L} \sum_{d_{n,l}=1}^{T} \Big[p(u_n = k) p(d_{n,l}) D_{n,l,k} \gamma_l^{-1} \int_0^{\infty} F_{n,l,k}(\omega_{n,l}, d_{n,l}) d\omega_{n,l}\Big]. \quad (15)$$

The resulting integral with respect to $\omega_{n,l}$ in (15) can be numerically approximated with a quadrature method. The matched filter in (14) can be computed with $\mathcal{O}(T \log T)$ using the fast Fourier transform (FFT) leading to an overall complexity of the integral per-pixel in (15) given by $\mathcal{O}(KLJT \log T)$, where K is the number of classes considered, L is the number of wavelengths, J is the computational cost of the evaluated integrand and T is the number of the temporal bins.

B. Depth estimation

The depth estimate can be obtain as follows

$$\hat{d}_n = \max_{d=1:T} p(d_n \,|\, \boldsymbol{Y_n}) \tag{16}$$

where

$$p(d_n|\boldsymbol{Y_n}) = \sum_{k=1}^{K} \prod_{l=1}^{L} \Big[p(u_n = k) p(d_n) D_{n,l,k} \gamma_l^{-1} \int_0^{\infty} F_{n,l,k}(\omega_{n,l}, d_n) d\omega_{n,l} \Big]. \tag{17}$$

Although ω can be marginalized from equation (17), this might lead to a high computational cost. In this paper, we choose to estimate the depth given the easily computed marginal map estimate $\omega_{n,l}^{\text{map}}$ using the simplified model introduced in Section IV-A, leading to

$$\hat{d}_n = \max_{d=1:T} p(d_n \,|\, \boldsymbol{Y_n}, \boldsymbol{\omega}_n^{\text{map}}). \tag{18}$$

The proposed approach allows the evaluation of the full marginal depth posterior. In addition to depth point estimate, this distribution will allow uncertainty quantification (i.e., quantify our confidence regarding the estimates). In this paper, we evaluate the depth uncertainty by considering the depth negative log-cumulative marginal posterior around the MAP estimate, i.e., NCD $= -\log \Big[\sum_{\hat{d}_n - \epsilon}^{\hat{d}_n + \epsilon} p(d_n \,|\, \boldsymbol{Y_n}, \boldsymbol{\omega}_n^{\text{map}}) \Big]$, where ϵ is a user fixed constant. Note that a small NCD indicates a high confidence about the estimate, while a large one would be an indication of low confidence.

V. Experimental results

In this section, we will evaluate the performance of the classification algorithm using the real multispectral single-photon Lego data used in [19] (see Fig. 1). This target has three classes of interest ($K = 3$) whose spectral signatures (related to $\boldsymbol{\alpha^r}$ and $\boldsymbol{\beta^r}$) are extracted from pixels acquired considering a negligible background contribution and after maximum acquisition time per-pixel (see signatures in Fig.1). α_l^b and β_l^b are relatively non-informative such that $(\alpha_l^b, \beta_l^b) = (1, \frac{T}{r_l^M})$ with r_l^M being the average number of signal photons per pixel for the l_{th} spectral wavelength. Two experiments have been performed. First, we consider a spatially sub-sampled data to analyse the behavior of the algorithm w.r.t. SBR and photons levels. The subsampled data has $N = 40 \times 40$ pixels, $L = 4$ wavelengths and $T = 1500$ time bins (bin width of 2ps), and is corrupted so that the SBR varies from 0.01 to 100. The object, of size 42 mm tall and 30 mm wide, was scanned with a 40ms acquisition time per pixel and per wavelength (total of 160ms per pixel) at a standoff distance of 1.8m with the IRF $g_l(.)$ depicted in Fig. 1 (the reader is advised to consult [19] for more details). Considering the foregoing parameters and for maximum acquisition time, the average computational time per-pixel of the proposed algorithm is $\approx$ 55ms using Matlab 2020a on a Intel Core i7-8700@3.2GHz, 16 GB RAM. Fig. 3 top and bottom represent, respectively, the root mean square error (RMSE) in meters defined by RMSE $= \sqrt{\frac{1}{N} ||\boldsymbol{d}^{\text{ref}} - \widehat{\boldsymbol{d}}||^2}$, where $\boldsymbol{d}^{\text{ref}}$ is obtained from sampling the whole scene with the maximum acquisition time and under a negligible background illumination, and the accuracy (ACC $= \frac{TP+TN}{TP+TN+FP+FN}$) w.r.t SBR and the average signal photons, where TP, TN, FP and FN represent respectively: true positive, true negative, false positive and false negative. These two figures provide the user with the required number of useful photons (which is proportional to the scanning time) needed to have a given depth precision and accuracy for different SBR levels.

The second experiment shows the obtained results when considering the full 200×200 pixels data. Fig. 2 represents (from left to right) the depth estimate, the class estimate and depth uncertainty measure w.r.t acquisition time per-pixel and per-wavelength and for Lego data in absence of background illumination (i.e., $SBR = \omega = 66$) and high illumination background where the SBR is as low as $\omega = 1.3$. These figures exhibit qualitatively the robustness of the proposed algorithm. Fig. 2(c) represents the NCD for $\epsilon = 1.5$mm where higher values indicate low-confidence regions. It is observed that higher depth uncertainty is observed for lower acquisition time data, and for low photon regions (e.g., black mouth and eyes, curved surfaces, etc).

VI. Conclusions

This paper has presented a new fast approach that performs depth estimation and class detection for multispectral LiDAR data which shows robustness even under challenging background illumination. In addition to the class and depth estimates, the proposed algorithm also provides the uncertainty measure associated with each parameter of interest. Besides being able to classify a scene w.r.t to defined spectral signatures, this algorithm can also complete a target detection task where objects of interest are materials with a specific spectral signature. This enables detecting objects which have a particular spectral signature under turbid media, e.g., metallic object detection underwater. Despite assuming one surface per-pixel, this algorithm can be used as a pre-processing step for multiple-surface-per-pixel to discard irrelevant pixels. Future work will investigate the use of this algorithm within an adaptive sampling strategy to improve Lidar data acquisition.

Acknowledgements

This work was supported by the UK Royal Academy of Engineering Research Fellowship Scheme (RF/201718/17128), and EPSRC Grants EP/T00097X/1, EP/S000631/1, EP/S026428/1, the Dasa project DSTLX1000147844 and the MOD University Defence Research Collaboration (UDRC) in Signal Processing.

References

[1] A. M. Wallace, A. Halimi, and G. S. Buller, "Full waveform lidar for adverse weather conditions," *IEEE Transactions on Vehicular Technology*, vol. 69, no. 7, pp. 7064–7077, 2020.

[2] A. M. Wallace, A. McCarthy, C. J. Nichol, X. Ren, S. Morak, D. Martinez-Ramirez, I. H. Woodhouse, and G. S. Buller, "Design and evaluation of multispectral lidar for the recovery of arboreal parameters," *IEEE Transactions on Geoscience and Remote Sensing*, vol. 52, no. 8, pp. 4942–4954, 2013.

[3] A. McCarthy, R. J. Collins, N. J. Krichel, V. Fernández, A. M. Wallace, and G. S. Buller, "Long-range time-of-flight scanning sensor based on high-speed time-correlated single-photon counting," *Applied optics*, vol. 48, no. 32, pp. 6241–6251, 2009.

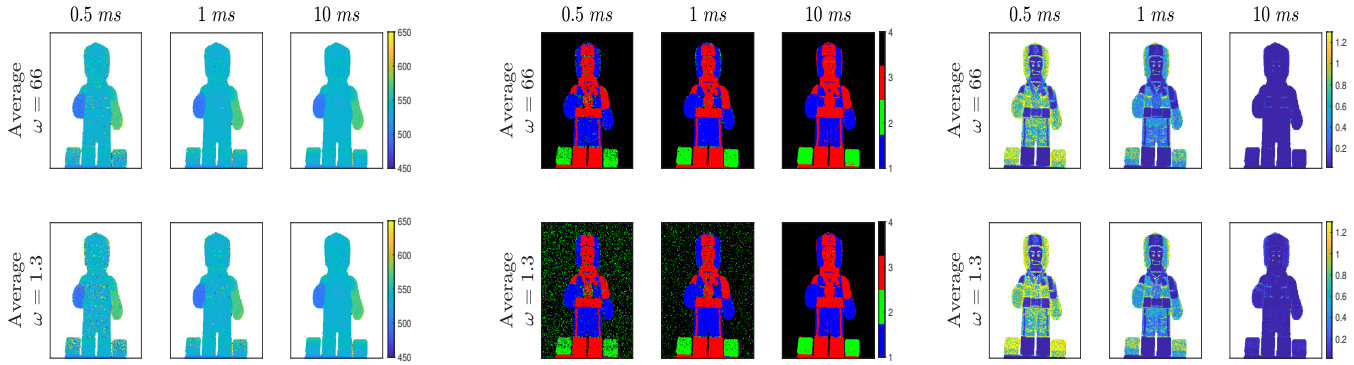

(a) Depth maps (b) Estimated classification maps (c) Estimated depth uncertainty

Fig. 2. Results of the proposed algorithm for different acquisition times and two SBR levels. (a) estimated depth maps (white pixels indicate no depth), (b) estimated classes, (c) the negative-log cumulative density (NCD) for $\epsilon = 1.5$mm (large values indicate high uncertainty).

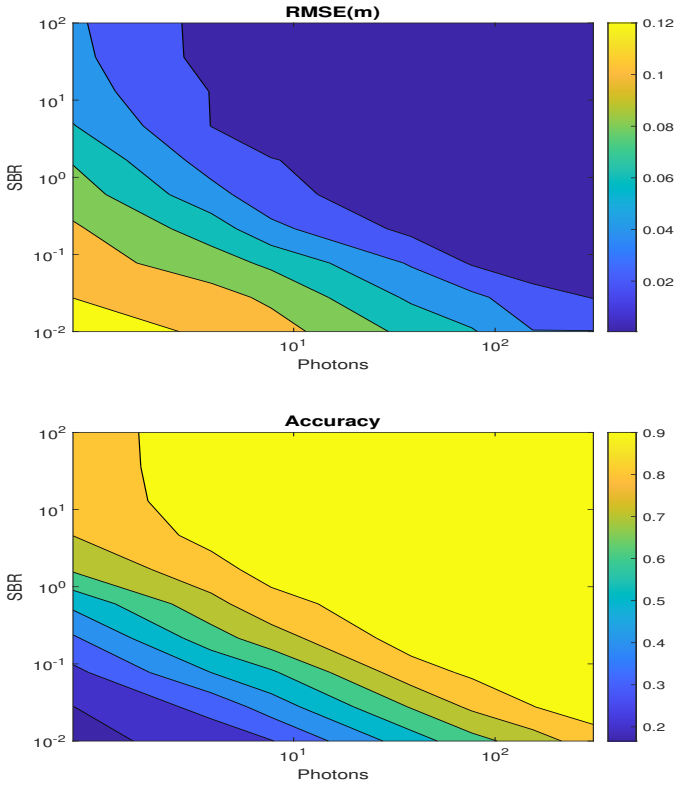

Fig. 3. Depth RMSEs (up) and Classification accuracy (down) of the sub-sampled lego data ($N = 40 \times 40$, $T = 1500$, $L = 4$, $K = 3$) w.r.t. signal-to-background ratio (SBR) and the average signal photons per pixel and per wavelength.

[4] A. M. Pawlikowska, A. Halimi, R. A. Lamb, and G. S. Buller, "Single-photon three-dimensional imaging at up to 10 kilometers range," *Optics express*, vol. 25, no. 10, pp. 11 919–11 931, 2017.

[5] Z. Li, E. Wu, C. Pang, B. Du, Y. Tao, H. Peng, H. Zeng, and G. Wu, "Multi-beam single-photon-counting three-dimensional imaging lidar," *Optics express*, vol. 25, no. 9, pp. 10 189–10 195, 2017.

[6] A. Maccarone, A. McCarthy, X. Ren, R. E. Warburton, A. M. Wallace, J. Moffat, Y. Petillot, and G. S. Buller, "Underwater depth imaging using time-correlated single-photon counting," *Optics express*, vol. 23, no. 26, pp. 33 911–33 926, 2015.

[7] A. Halimi, A. Maccarone, A. McCarthy, S. McLaughlin, and G. S. Buller, "Object depth profile and reflectivity restoration from sparse single-photon data acquired in underwater environments," *IEEE Transactions on Computational Imaging*, vol. 3, no. 3, pp. 472–484, 2017.

[8] G. Satat, M. Tancik, and R. Raskar, "Towards photography through realistic fog," in *2018 IEEE International Conference on Computational Photography (ICCP)*. IEEE, 2018, pp. 1–10.

[9] Y. Altmann, A. Maccarone, A. Halimi, A. McCarthy, G. Buller, and S. McLaughlin, "Efficient range estimation and material quantification from multispectral lidar waveforms," in *2016 Sensor Signal Processing for Defence (SSPD)*. IEEE, 2016, pp. 1–5.

[10] A. Halimi, R. Tobin, A. McCarthy, J. Bioucas-Dias, S. McLaughlin, and G. S. Buller, "Robust restoration of sparse multidimensional single-photon lidar images," *IEEE Transactions on Computational Imaging*, vol. 6, pp. 138–152, 2019.

[11] J. Tachella, Y. Altmann, M. Márquez, H. Arguello-Fuentes, J.-Y. Tourneret, and S. McLaughlin, "Bayesian 3d reconstruction of subsampled multispectral single-photon lidar signals," *IEEE Transactions on Computational Imaging*, vol. 6, pp. 208–220, 2019.

[12] A. Halimi, A. Maccarone, R. Lamb, G. S. Buller, and S. McLaughlin, "Robust and guided bayesian reconstruction of single-photon 3d lidar data: Application to multispectral and underwater imaging," *arXiv preprint arXiv:2103.10122*, 2021.

[13] Y. Altmann, A. Maccarone, A. McCarthy, G. Buller, and S. McLaughlin, "Joint range estimation and spectral classification for 3d scene reconstruction using multispectral lidar waveforms," in *2016 IEEE Statistical Signal Processing Workshop (SSP)*. IEEE, 2016, pp. 1–5.

[14] Y. Altmann, A. Maccarone, A. McCarthy, G. Newstadt, G. S. Buller, S. McLaughlin, and A. Hero, "Robust spectral unmixing of sparse multispectral lidar waveforms using gamma markov random fields," *IEEE Transactions on Computational Imaging*, vol. 3, no. 4, pp. 658–670, 2017.

[15] J. Tachella, Y. Altmann, S. McLaughlin, and J.-Y. Tourneret, "On fast object detection using single-photon lidar data," in *Wavelets and Sparsity XVIII*, vol. 11138. International Society for Optics and Photonics, 2019, p. 111380T.

[16] A. Halimi, A. Wallace, G. S. Buller, and S. McLaughlin, "Fast surface detection using single-photon detection events," in *2020 Sensor Signal Processing for Defence Conference (SSPD)*. IEEE, 2020, pp. 1–5.

[17] S. Hernandez-Marin, A. M. Wallace, and G. J. Gibson, "Bayesian analysis of lidar signals with multiple returns," *IEEE Transactions on Pattern Analysis and Machine Intelligence*, vol. 29, no. 12, pp. 2170–2180, 2007.

[18] J. Rapp and V. K. Goyal, "A few photons among many: Unmixing signal and noise for photon-efficient active imaging," *IEEE Trans. Comput. Imaging*, vol. 3, no. 3, pp. 445–459, Sept. 2017.

[19] R. Tobin, Y. Altmann, X. Ren, A. McCarthy, R. A. Lamb, S. McLaughlin, and G. S. Buller, "Comparative study of sampling strategies for sparse photon multispectral lidar imaging: towards mosaic filter arrays," *Journal of Optics*, vol. 19, no. 9, p. 094006, 2017.

[20] Y. Altmann, X. Ren, A. McCarthy, G. S. Buller, and S. McLaughlin, "Robust bayesian target detection algorithm for depth imaging from sparse single-photon data," *IEEE Transactions on Computational Imaging*, vol. 2, no. 4, pp. 456–467, 2016.